Available online at www.sciencedirect.com
SCIENCE DIRECT®
Acta Materialia 53 (2005) 247–254
Acta MATERIALIA
www.actamat-journals.com

Faceting of Σ3 and Σ9 grain boundaries in Cu–Bi alloys

B.B. Straumal [a,*], S.A. Polyakov [a,b], E. Bischoff [b], W. Gust [b], B. Baretzky [b]

[a] *Laboratory of Interfaces in Metals, Institute of Solid State Physics, Institutskii prospect 15, 142432 Chernogolovka, Moscow District, Russia*
[b] *Max-Planck-Institut für Metallforschung and Institut für Metallkunde, Heisenbergstr. 3, 70569 Stuttgart, Germany*

Received 11 March 2004; received in revised form 11 August 2004; accepted 13 August 2004

Abstract

The faceting of Σ3 and Σ9 tilt grain boundaries (GBs) has been studied in bicrystals of pure Cu and Cu–Bi alloys containing 2.5×10^{-3}, 10×10^{-3} and 16×10^{-3} at.% Bi. The Σ3(100), Σ9(100), Σ9(−110), and Σ9(−120) facets and non-CSL Σ3 82° 9R facet were observed, where Σ is the inverse density of coincidence sites. The ratio between GB energy, σ_{GB}, and surface energy, σ_{sur}, was measured by atomic force microscopy using the GB thermal-groove method. The GB energy and thermal-groove deepening rate increased slightly between 0 and 10×10^{-3} at.% Bi for all facets studied. However, between 10×10^{-3} and 16×10^{-3} at.% Bi the GB energy increased dramatically [from a factor 2 for the Σ9(110) facet to 15 times larger for the Σ3(100) facet]. The thermal-groove deepening rate also increased by a factor of 10 in this concentration range. This change corresponds well with the GB solidus line (i.e., the formation of a stable layer of a liquid-like GB phase called GB prewetting) observed previously. Wulff diagrams were constructed using measured σ_{GB}/σ_{sur} values.

Keywords: Grain boundaries; Faceting; Roughening; Cu; Cu–Bi alloys; Prewetting; Phase diagrams

1. Introduction

The faceting of low-Σ grain boundaries (GBs), where Σ is the inverse density of coincidence sites, plays a special role in polycrystals. In certain materials the number of low-Σ GBs, especially Σ3 and Σ9 GBs, is surprisingly high [1]. An increase in Σ3 and Σ9 GBs is accompanied by a marked improvement of the properties, particularly a decrease in GB corrosion rate [2]. Faceting is a characteristic feature for GBs with misorientation angles close to the coincidence misorientation, θ_Σ. The presence of GB faceting correlates also with the phenomenon of abnormal grain growth [3]. Faceting may be regarded as a phase transition in which a flat (single phase) interface is transformed into a faceted structure consisting of two or more facet types (phases) which coexist along the line of intersection [4].

Another important class of GB phase transformations are GB wetting, prewetting, and premelting transitions, which can drastically change the properties of polycrystals, especially those of nanocrystalline materials. If a GB wetting phase transition proceeds during heating within the two-phase liquid + solid area of the bulk phase diagram (Fig. 1), then the liquid phase forms at the GBs, and replaces them completely since the GB cannot exist in the equilibrium with the melt. The GB solidus in the single-phase S area may be regarded as a continuation of the GB wetting tie-lines which are present in the two-phase liquid + solid area. The GB solidus line is defined as labeled in Fig. 1. GB properties such as GB diffusivity, segregation, mobility, brittleness, plasticity, and electrical conductivity change drastically at GB solidus ([5] and references therein).

* Corresponding author. Tel.: +7 09652 22957; fax: +7 095 2382326/1117067.
E-mail address: straumal@issp.ac.ru (B.B. Straumal).

1359-6454/$30.00 © 2004 Acta Materialia Inc. Published by Elsevier Ltd. All rights reserved.
doi:10.1016/j.actamat.2004.08.015

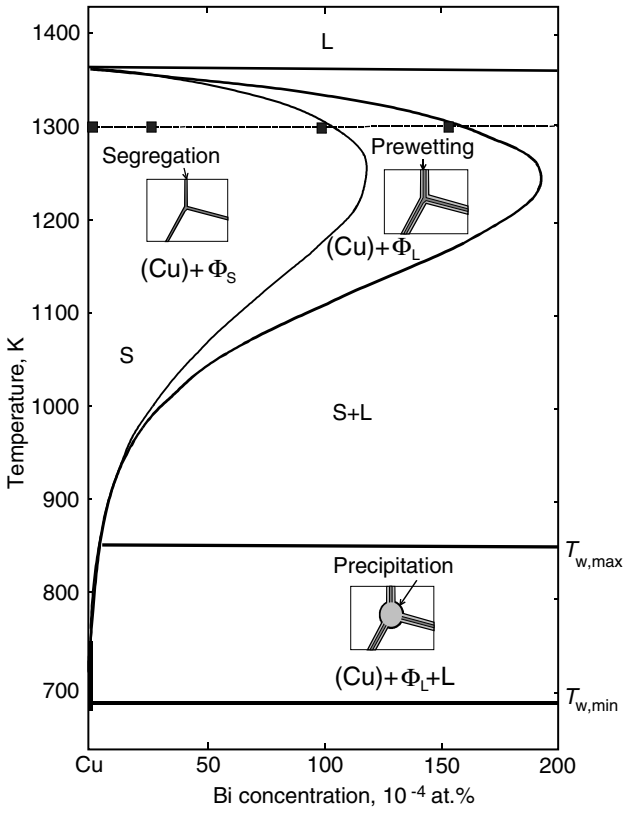

Fig. 1. Cu-rich side of the Cu–Bi phase diagram. The thick curve is the (retrograde) bulk solidus line [7]. The thin retrograde curve is the GB solidus line obtained for the Cu–Bi polycrystals [7]. The GB wetting phase transition tie-lines at $T_{w,max}$ and $T_{w,min}$ in the two-phase S + L area are constructed from the data of [15]. The broken line denotes the annealing temperature of 1293 K. The black squares denote the Bi concentration in the samples (0, 25, 100 and 160 at.ppm Bi).

The discontinuity of the temperature dependence of the GB energy at the GB solidus line in the Cu–Bi system reveals a first order GB prewetting (premelting) phase transition [6]. The coupling of GB faceting and wetting–prewetting phase transitions is of primary importance since it can influence interface-controlled processes in two- and multicomponent polycrystals, like superplasticity, liquid-phase and activated sintering, liquid phase penetration, welding, soldering, penetration of melts and fluids in rocks, etc. [5]. Cu–Bi alloys present a good opportunity to study this coupling since the formation of GB phases was studied recently [5–7], and the influence of Bi additions on GB faceting in Cu is also well documented in the literature [8–10].

2. Experimental details

For the investigation of GB faceting, a cylindrical, coaxial Cu bicrystal was grown by the Bridgman technique from 99.999 wt% purity Cu [11]. Grain 1 is completely surrounded by a grain 2 and a Σ9 [1 1 0] tilt GB formed between them. The (1 1 1)/(1 1 5) inclination of the Σ9 GB is unstable against the dissociation reaction: $\Sigma 9 \rightarrow \Sigma 3 + \Sigma 3$. Therefore, multiple elongated twins (Fig. 2) with well-developed Σ3 GBs appear during the growth of a bicrystal instead of $\{1\,1\,1\}_1$ /$\{1\,1\,5\}_2$ or Σ9(1 1 0) facets (the subscripts 1 and 2 correspond to the grains 1 and 2) [5]. The [1 1 0] axes in both grains are parallel to the growth axis. Therefore, the Σ3 [1 1 0] tilt GB in the sample contains all crystallographically possible inclinations. 2.5 mm thick circular platelets were cut from the bicrystal perpendicularly to the growth axis and etched. Next, the vapor transfer method was used to introduce Bi into the Cu platelets.

Different annealing times for a vapor transfer from a Cu–0.3 at.% Bi alloy vapor source were chosen in order to produce samples with different Bi content (2.5×10^{-3}, 10×10^{-3} and 16×10^{-3} at.% Bi). All samples were homogenized at 1123 K for 168 h in evacuated (5×10^{-4} Pa) silica ampules without a Bi source. The alloyed and pure platelets were annealed then in a 80% Ar + 20% H_2 gas mixture at 1293 K and 2×10^4 Pa for 48 h. During the annealing the GB migrates slowly towards the center of the bicrystal permitting equilibrium facets to develop. The GB shape and geometry of facets were analyzed and photographed in polarized light in bright and dark field with the aid of a Zeiss Axiophot optical microscope and by a Topometrix 2000 Explorer atomic force microscope operating in the contact mode. The samples were then carefully repolished and annealed again for 48 h to form GB thermal grooves.

In order to determine the ratio between GB energy, σ_{GB}, and surface energy, σ_{sur}, the profiles of the GB thermal grooves were analyzed with the aid of atomic force microscopy (AFM). Typically, a 50 μm × 50 μm field containing 500 × 500 pixels was analyzed. For the analysis, 10 neighboring profiles were used to obtain a

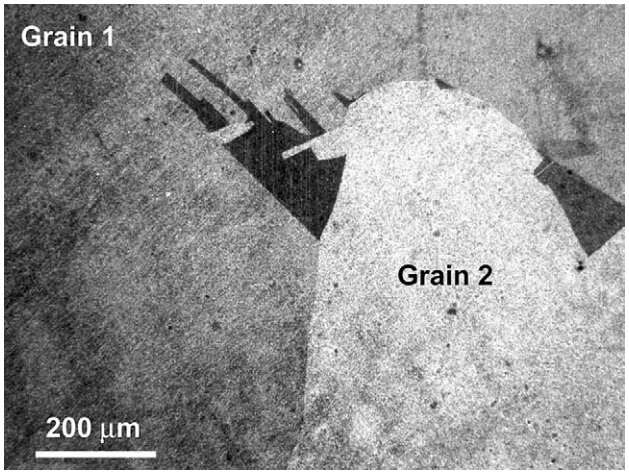

Fig. 2. Micrograph of multiple twins between grain 1 and grain 2 with Σ9 misorientation. The common [1 1 0] axis is perpendicular to the micrograph plane.

mean profile (Fig. 3). The diameter of the individual experimental points shown in Fig. 3 is larger than the error of AFM height measurements. The σ_{GB}/σ_{sur} ratio was calculated using the measured values for the GB groove angles. To determine the groove angle, full groove profile was used for pure Cu and Cu with 2.5×10^{-3} and 10×10^{-3} at.% Bi (Figs. 3(a)–(c)) as proposed in [6]. These profiles can be good approximated by the standard Mullins solution. The profile part from one "Mullins hillock" to another one containing about 250–300 experimental points was used for the fitting. The AFM needle used is very fine. Therefore, only 2–4 experimental points at the groove tip had to be excluded from the fitting procedure. Before the AFM method became available, the GB groove profiles were measured using the optical interferometer. In those measurements the distorted area at the groove tip, not usable for the fitting, was about five times larger ([12] and references therein). Each side of the GB groove profile was fitted separately and the tip location was calculated [6]. Polynoms of first, second, fourth, sixth and eighth order were compared. The transition from first to fourth order improved the results drastically. Since further extension of polynoms did not change the results, the fourth order polynoms were used for the approximation. The derivatives for both halves of the groove profile were determined in the intersection point. Their sum delivered the groove angle. For Cu containing 16×10^{-3} at.% Bi the GB groove was very deep, asymmetric and faceted (Fig. 3(d)). Since it cannot be approximated by the Mullins solution, the groove tip angle was measured in a linear approximation. The local misorientation was determined with a commercially available system (OIM™, by TSL). The deviation of misorientation angle from ideal Σ3 and Σ9 misorientations was below 2°.

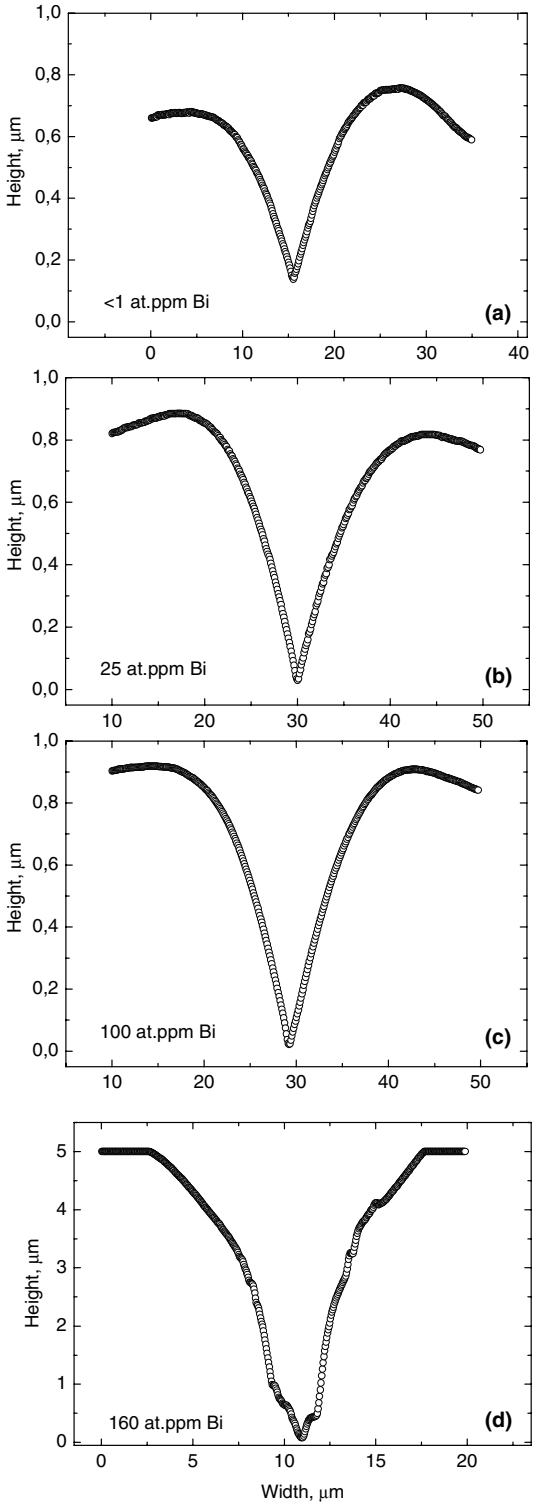

Fig. 3. AFM profiles of the thermal groove for the Σ9(−1 1 0) facet at various Bi concentrations. Note the different height scale for 160 at.ppm Bi.

3. Results

The Cu–Bi phase diagram is shown in Fig. 1. The thick curve is the (retrograde) bulk solidus line [7]. The thin retrograde curve is the GB solidus line obtained in Cu–Bi polycrystals [7]. To the left of the GB solidus the conventional segregation layer Φ_S is present in GBs. The GB prewetting phase transition occured at the GB solidus line and a thin layer of the Bi-rich GB phase Φ_L formed in between the GB and bulk solidus lines [7]. The occurrence of GB Bi-rich layer between the GB and bulk solidus lines was observed by high-resolution electron microscopy (HREM) [13,14]. Computer modeling also revealed that specific interfacial phases form in the Cu–Bi system [14]. The GB wetting phase transition tie-lines at $T_{w,max}$ and $T_{w,min}$ in the two-phase solid + liquid area are constructed based on the data [15]. Above $T_{w,max}$ all high-angle GBs are wetted by the melt. Below $T_{w,min}$ no GB wetting occurs in two-phase (Cu) + L polycrystals. Above the GB wetting tie-line the energy of two solid/liquid interfaces $2\sigma_{SL}$ is lower than the GB energy σ_{GB}. The resulting energy gain

$\Delta\sigma = 2\sigma_{SL} - \sigma_{GB}$ is also present in the one-phase area of the bulk phase diagram where only the solid solution is in equilibrium. The energy difference, $\Delta\sigma$, can stabilize a thin GB layer with a thermodynamically defined liquidus composition in the single-phase area (Fig. 1). As a result, a tie-line of the GB wetting phase transition can continue in the S area of the bulk phase diagram. The broken line in Fig. 1 denotes the annealing temperature of 1293 K. The black squares denote the Bi concentration in the samples (0, 2.5×10^{-3}, 10×10^{-3} and 16×10^{-3} at.% Bi). Three samples (0, 2.5×10^{-3} and 10×10^{-3} at.% Bi) were in the (Cu) + Φ_S area, and one sample with 16×10^{-3} at.% Bi was between the GB and bulk solidus lines.

At temperature $T = 1293$ K $= 0.95T_m$ the Σ3 GB contains two facets, namely symmetric Σ3 twins [$(111)_1/(111)_2$ or Σ3(100) facets] and non-CSL facets forming the angle of 82° with the Σ3(100) facets. Therefore, the twin plates in Cu are not rectangular. HREM studies revealed that this 82° facet has a so-called 9R structure forming a plate of body-centered cubic GB phase in the face-centered cubic matrix [12]. Such Σ3(100) and 82° 9R facets on the Σ3 twin plate are also clearly seen in our samples in Fig. 2. The same two Σ3(100) and 82° 9R facets are present at $T = 1293$ K in alloys with 2.5×10^{-3}, 10×10^{-3} and 16×10^{-3} at.% Bi. No additional facets appear at $T = 1293$ K both in (Cu) + Φ_S and (Cu) + Φ_L areas of the Cu–Bi phase diagram. The $(111)_1/(115)_2$ or Σ9(110) facets are unstable against the dissociation reaction: Σ9 → 2Σ3 at all Bi concentrations studied. Σ9 GBs in pure Cu contain two CSL facets Σ9(−110) and Σ9(−120) at $T = 1293$ K. These facets are present at all Bi concentrations studied. Two additional CSL facets Σ9(−410) and Σ9(−230) appear at the highest Bi concentration of 16×10^{-3} at.%. This corresponds to the observation that the fraction of faceted GBs in polycrystals increases with increased Bi content [8–10]. The Σ9(100) facet becomes stable in pure Cu between 0.8 and $0.95T_m$ [11]. It also becomes stable in Cu–Bi alloys between 10×10^{-3} and 16×10^{-3} at.% Bi. Nevertheless, it was possible to measure the GB groove shape at $0.95T_m$ for low Bi concentrations at the inclination angle corresponding to the Σ9(100) facet, where the GB is only slightly curved.

The AFM profiles of the thermal groove at the Σ9(−1,1,0) facet at various Bi concentrations are shown in Fig. 3. At 0, 2.5×10^{-3} and 106×10^{-3} at.% Bi. [i.e. in the (Cu) + Φ_S area of the Cu–Bi phase diagram] the groove profiles correspond to the Mullins equations when groove growth is surface diffusion controlled. At 16×10^{-3} at.% Bi in the (Cu) + Φ_L area of the Cu–Bi phase diagram the shape of GB groove changes drastically, (Fig. 3(d)) becoming very deep (about 5 μm instead of 0.6–0.9 μm at low Bi concentrations), asymmetric, and faceted. The groove penetration rate along GB drastically increases in the (Cu) + Φ_L area of the Cu–Bi phase diagram in comparison with (Cu) + Φ_S area (Fig. 4). This means that the presence of GB phase between GB and bulk solidus lines enhances the kinetics of GB grooving.

The dependence of the σ_{GB}/σ_{sur} ratio on the bulk Bi concentration for (a) Σ3(100) and 9R Σ3 facets and (b) Σ9(100), Σ9(−110) and Σ9(−120) facets is shown in Fig. 5. The Σ9(100) facet flattens only between 10×10^{-3} and 16×10^{-3} at.% Bi. Therefore, the GB groove shape at low Bi concentrations has been meas-

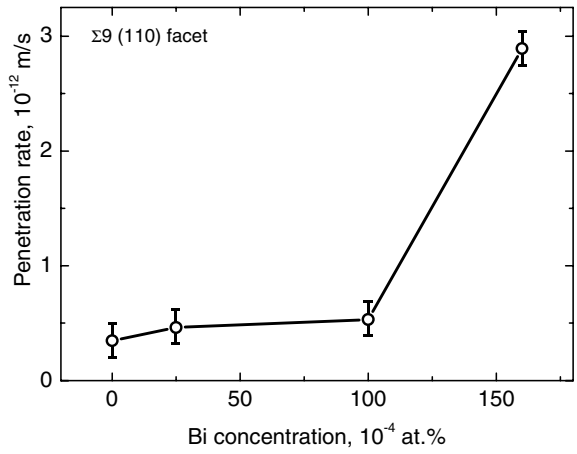

Fig. 4. Dependence of the groove penetration rate on the bulk Bi concentration for the Σ9(110) facet.

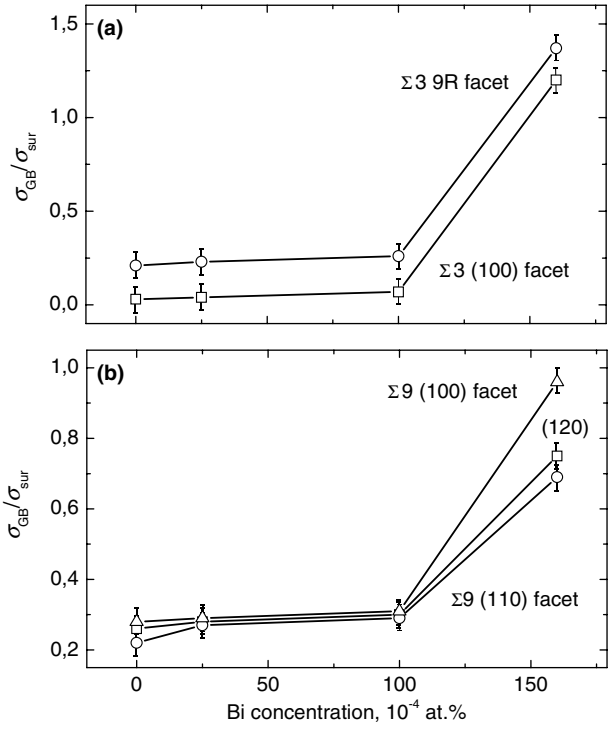

Fig. 5. Dependence of ratio σ_{GB}/σ_{sur} on bulk Bi concentration for (a) Σ3(100) and 9R Σ3 facets and (b) Σ9(100), Σ9(−110) and Σ9(−120) facets.

ured at the inclination angle corresponding to the facet Σ9(100) on the slightly curved GB. In all five cases the addition of Bi (up to 10×10^{-3} at.% Bi), i.e. in the one-phase S area slightly increases the σ_{GB}/σ_{sur} ratio. However, the σ_{GB}/σ_{sur} ratio increased drastically after intersection of the GB solidus line between 10×10^{-3} and 16×10^{-3} at.% Bi. The σ_{GB}/σ_{sur} value increases by a factor of 15 for symmetric twin GBs Σ3(100), and by a factor of 3 for the Σ9(100) facet.

4. Discussion

In the case of ordinary coexistence of two bulk phases a large inclusion of one phase may remain in stable equilibrium inside of the second phase (matrix). The average shape of the inclusion is then determined by strictly thermodynamic considerations based on the Gibbs energy minimum for the creation of the necessary interfacial boundary. If both coexisting phases are isotropic (e.g. fluids), the shape of the inclusion is spherical. If one or both are crystalline or otherwise anisotropic, interfaces of some orientations are preferred over those of the other orientations, and the "equilibrium crystal shape" (ECS) of the inclusion is non-spherical and can exhibit varying complexity. Wulff first proposed the following construction (see Fig. 6(a)) [16]. When the interface Gibbs energy per unit area $f(\boldsymbol{m})$ is drawn as a polar plot (Wulff plot sometimes called γ-plot), the crystal shape is given as the interior envelope of the family of perpendicular planes passing through the end of radius vectors $\boldsymbol{m}$. Such a crystal shape corresponds to the minimum of the Gibbs energy. Andreev [17] first pointed out that the Wulff construction is simply the geometrical version of a two-dimensional Legendre transformation between the Gibbs energy, $f(\boldsymbol{m})$, and the crystal shape, $r(\boldsymbol{h})$, where $\boldsymbol{h}$ is the facet orientation relative to crystal axes. Thus, knowing the Gibbs energy one can reconstruct the equilibrium crystal shape and vice versa.

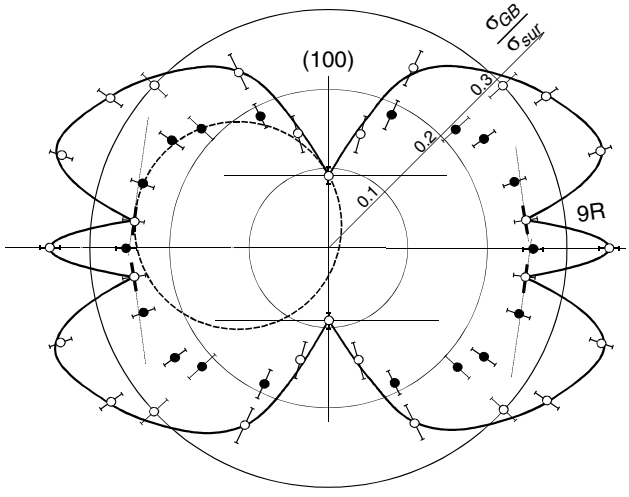

Fig. 6. Wulff diagram for [110] tilt Σ3 GBs in Cu at 1273 K constructed using the data [12]. Open circles denote the ratio σ_{GB}/σ_{sur} of non-relaxed GBs with different inclinations produced by diffusion bonding. The solid circles denote σ_{GB}/σ_{sur} after relaxation (i.e. after decomposition into low-energy facets) The circles denote the scale of the σ_{GB}/σ_{sur} ratio.

Until now only anisotropic inclusion and isotropic second phase were considered. This corresponds to the crystal surfaces. What happens when both the "matrix" and "inclusion" are crystalline and, therefore, anisotropic? Grain boundaries as interfaces between two identical but misoriented lattices represent the simplest case. Therefore, the approach developed for description of ECS for crystal surfaces can also be used for GBs. If the flat surface (or interface) has an inclination between two energetic minima in Gibbs energy it would transform into a faceted structure consisting of two facet types (phases) which coexist along the lines of intersection [4]. The Wulff construction, that permits Gibbs energy estimation the energy of such faceted interfaces, would predict a circle between neighboring $f(\boldsymbol{m})$ minima. The Wulff diagram for [110] tilt Σ3 GBs in Cu at 1273 K is shown in Fig. 6 constructed using the data ([12] and references therein). Open circles denote the ratio σ_{GB}/σ_{sur} of non-relaxed GBs with different inclinations produced by diffusion bonding. Solid circles denote σ_{GB}/σ_{sur} after relaxation (i.e. after decomposition into low-energy facets). Solid circles are positioned along the circle segments drawn between the minima for the Σ3(100) and 82° 9R facets. The circles denote the scale of the σ_{GB}/σ_{sur} ratio.

The Wulff plot is shown in Fig. 7(a) for Σ3 GBs at 1293 K and 10×10^{-3} at.% Bi constructed using the σ_{GB}/σ_{sur} ratios measured with the aid of AFM (see Fig. 5). The low energy of coherent Σ3(100) facets determines the platelet-like form of twins in Cu. However, the difference between σ_{GB}/σ_{sur} values for Σ3(100) and 82° 9R facets is only about 15% at 16×10^{-3} at.% Bi and, therefore, the ECS for twin becomes broader and less like the platelet. The inclination angle, $\phi(\boldsymbol{h})$, schematically shown in Fig. 7(a) determines the angular intervals for the of Σ3(100) and 82° 9R facets. Wulff plots are shown in Figs. 7(b) and (c) for Σ9 GBs at 2.5×10^{-3} and 10×10^{-3} at.% Bi. The Σ9(110) facet is unstable against the dissociation into two Σ3 GBs. Therefore, the point with doubled Σ3(100) energy appears at the Σ9 Wulff plot instead of the Σ9(110) facet energy. The point at inclination corresponding to the $(100)_{\Sigma9CSL}$ facet position has been measured at curved (rough) GB. No minima appeared in the $f(\boldsymbol{m})$ energy dependence at this inclination, since the Σ9(100) facet appears only at 16×10^{-3} at.% Bi. The Σ9(−120) facets are stable in pure Cu [11], but they become metastable at 2.5×10^{-3} and 10×10^{-3} at.% Bi. The presence of the Σ9(−120) facets in the sample reveal the existence of the energetic minima on the Wulff plot $f(\boldsymbol{m})$. However,

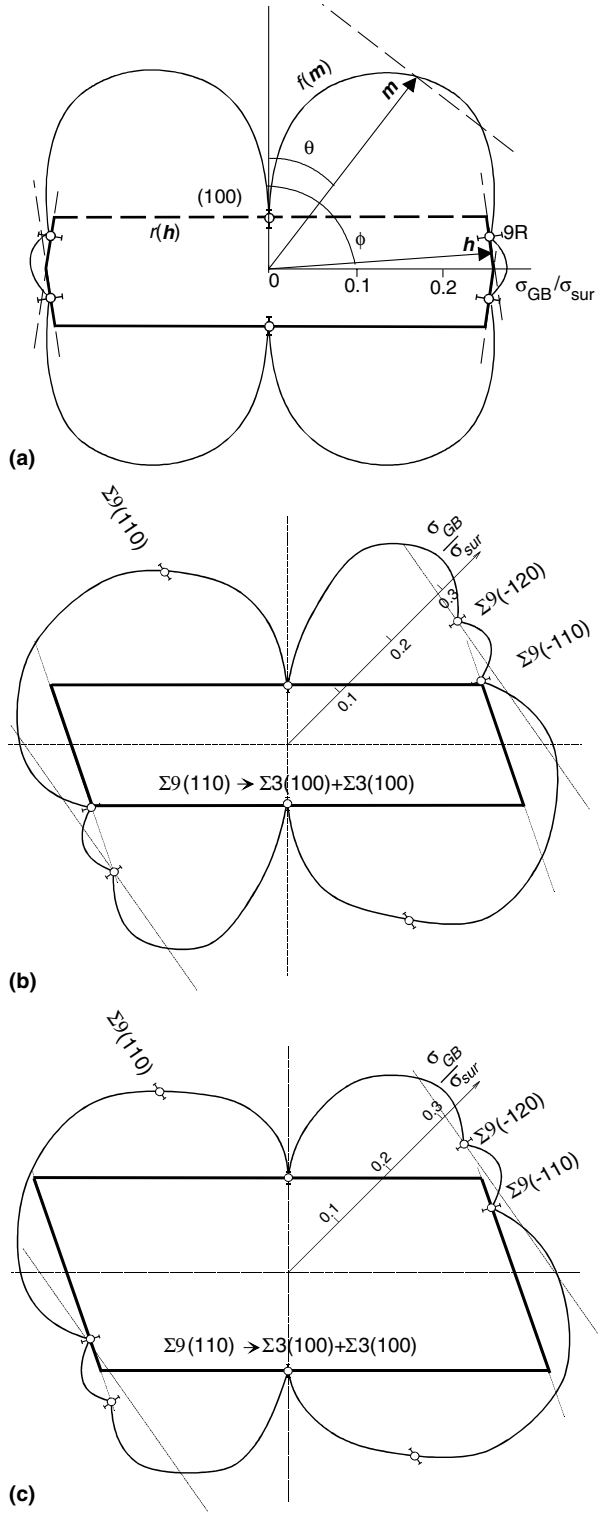

Fig. 7. Wulff energy $f(\boldsymbol{m})$ and resulting ECS $r(\boldsymbol{h})$ in a plane section perpendicular to the [1 1 0] tilt axis for the (a) Σ3 GBs in Cu–100 at.ppm Bi alloy; (b) Σ9 GBs in Cu–25 at.ppm Bi alloy and (c) Σ9 GBs in Cu–100 at.ppm Bi alloy. The open circles represent the GB energy σ_{GB} for various facets measured with the aid of AFM. The values σ_{GB}/σ_{sur} = 0.1, 0.2 and 0.3 are marked in polar coordinates. θ and ϕ are the angular variables which measure the interfacial orientation ($\boldsymbol{m}$) and crystal shape ($\boldsymbol{h}$), respectively.

it follows from Figs. 7(b) and (c) that these minima are not deep enough to allow the corresponding facets to be stable.

The theoretical picture of the thermal evolution of ECS for a typical crystal surrounded by the vacuum or fluid is given in [18]. As T increases, facets shrink and eventually disappear, each at its own characteristic roughening ("faceting") temperature $T_R(\boldsymbol{h})$. At sufficiently high temperatures the ECS becomes smoothly rounded everywhere (unless, of course, the system first undergoes a bulk phase change, such as melting). The observed Σ3(1 0 0)/82° 9R ridges of the twin plates are sharp. In other words, the roughening temperature T_R for Σ3(1 0 0) and 9R facets is higher than the melting temperature T_m. In case of Σ9 GBs the situation is more complicated. For example, the GB with an inclination corresponding to the Σ9(1 0 0) facet remains rough (rounded) at 0, 2.5×10^{-3} and 10×10^{-3} at.% Bi (Figs. 7(b) and (c)). However, between the lines of the GB and bulk solidus the Σ9(1 0 0) facet becomes flat, i.e. between 10×10^{-3} and 16×10^{-3} at.% Bi the GB roughening transition occurs for the Σ9(1 0 0) facet. However, the Wulff diagram shows that the Σ9(1 0 0) facet remains metastable at 16×10^{-3} at.% Bi. In other words, although a minimum is present on the $f(\boldsymbol{m})$ curve at the Σ9(1 0 0) inclination, this minimum remains too shallow to contribute to the ECS.

The phase diagram for Σ3 facets is shown in Fig. 8 for $\phi(\boldsymbol{h})$ according to the approach proposed in [18] for ECS. Instead of the temperature, the Bi concentration c is plotted as the ordinate. No fields corresponding to the rough phases are present in this diagram. Open

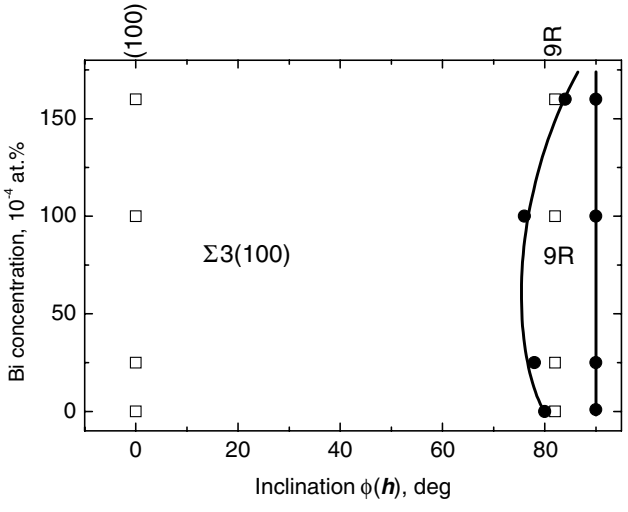

Fig. 8. Bi concentration vs. inclination for Σ3 [1 1 0] tilt GBs in Cu plotted according to the approach of [18]. The inclination ϕ is the angular variable which measures the crystal shape ($\boldsymbol{h}$) in an equatorial section of the full three-dimensional phase diagram which is perpendicular to the [1 1 0] tilt axis. The (c,ϕ) phase diagram plots the angular outline of the faceted areas of GB shape.

squares at $\phi = 0°$ and 82° denote the Σ3(1 0 0) and 9R facets observed at all studied Bi concentrations. If one intentionally produce a flat GB with intermediate inclination (for example, $\phi = 45°$) and than anneals it at $T = 0.95T_m$ the GB would decompose into the grid of Σ3(1 0 0) and 9R facets, as it was observed experimentally in [18]. Fig. 6 shows the Wulff diagram for this case. The lines in Fig. 8 mark the angular areas $\phi(\boldsymbol{h})$ for the ECS. The circles mark the ϕ values where Σ3(1 0 0) and 9R facets intersect. The same circles mark the ϕ values where 9R and 9R facets intersect. The ϕ values were obtained from the experimentally measured Wulff diagrams for different c values. The $9R/9R$ ridges lie at $\phi = 90°$. With increasing Bi concentration, c, the 9R area becomes broader at the cost of Σ3(1 0 0) area up to 10×10^{-3} at.% Bi. Between 10×10^{-3} and 16×10^{-3} at.% Bi the Σ3(1 0 0) area shrinks again.

The phase diagram for Σ9 facets is shown in Fig. 9 for $\phi(\boldsymbol{h})$, the c is plotted as the ordinate. Open squares denote the stable facets and crosses denote the metastable facets. The lines mark the the angular areas $\phi(\boldsymbol{h})$ for the respective ECS facets. With increasing c the Σ9(−4 1 0) area becomes broader on the cost of 2Σ3(1 0 0) areas up to 10×10^{-3} at.% Bi. Between 10×10^{-3} and 16×10^{-3} at.% Bi the Σ3(1 0 0) area shrinks and two new facets Σ9(−4 1 0) and Σ9(−2 3 0) appear. The facet Σ9(−1 2 0) becomes metastable between 0 and 2.5×10^{-3} at.% Bi. Therefore, the GB prewetting phase transition increases the number of stable Σ9 facets between 10×10^{-3} and 16×10^{-3} at.% Bi. This fact explains the early data obtained in the Cu–Bi polycrystals [9,10]. The number of faceted GBs in Cu–3×10^{-3} at.% Bi [10] and Cu–9×10^{-3} at.% Bi [9] polycrystalline alloys was low since the Bi content in these alloys is below the GB solidus concentration. However, the number of faceted GBs in Cu–30×10^{-3} at.% Bi alloys was very high [9] because this concentration is well above the GB solidus.

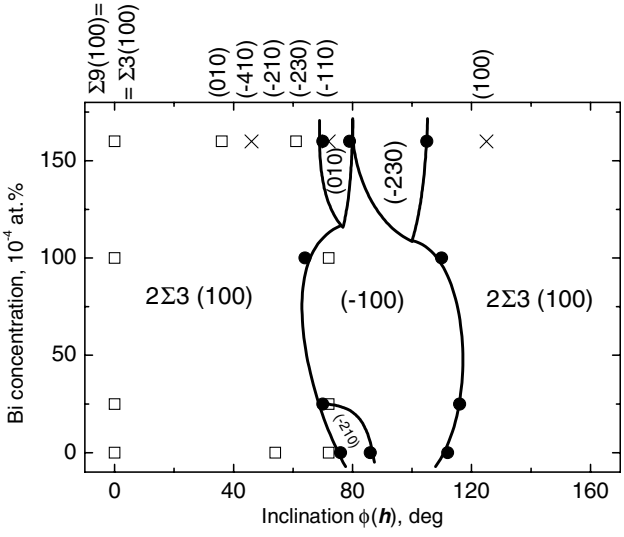

Fig. 9. Bi concentration vs. inclination for Σ9 [1 1 0] tilt GBs in Cu plotted according to the approach of [18].

5. Conclusions

1. Cylindrical tilt Σ3 and Σ9 GBs in Cu bicrystals containing the full spectrum of inclinations become faceted at $0.95T_m$ in the solid-solution area of the Cu–Bi phase diagram (i.e. from 0 to 16×10^{-3} at.% Bi).
2. No rough corners between Σ3(1 0 0) and 82° 9R facets were observed indicating that T_m is lower than the facets roughening temperature in pure Cu and Cu–Bi alloys.
3. The ratio between GB energy, σ_{GB}, and surface energy, σ_{sur}, was measured by atomic force microscopy using the GB thermal-groove method for tilt Σ3 and Σ9 GBs. Between 0 and 10×10^{-3} at.% Bi the σ_{GB}/σ_{sur} ratio and deepening rate of thermal groove slightly increased with increasing Bi concentration, c. By intersecting of the GB solidus line (about 11×10^{-3} at.% Bi), both σ_{GB}/σ_{sur} ratio and deepening rate of the thermal groove drastically increased.
4. Wulff diagrams constructed using the measured σ_{GB}/σ_{sur} values reveal that the Σ9(−1 2 0) facet that is stable at low c values becomes metastable at high c values. On the contrary, the Σ9(1 1 0) facet which is rough (unstable) at low c values becomes metastable at high c values.

Acknowledgements

Investigations were partly supported by the German Federal Ministry for Education and Research (project WTZ RUS 04/014), INTAS (contract 03-51-3779), Russian Foundation for Basic Research RFBR (contract 04-03-32800) and NATO Linkage grant (contract PST.CLG.979375).

References

[1] Harada K, Tsurekawa S, Watanabe T, Palumbo G. Scr Mater 2003;49:367.
[2] Shimada M, Kokawa H, Wang ZJ, Sato YS, Karibe I. Acta Mater 2002;50:2331.
[3] Lee SB, Yoon DY, Henry MF. Acta Mater 2000;48:3071.
[4] Cahn JW. J Phys 1982;43(12):C6-199.
[5] Straumal BB, Baretzky B. Interface Sci 2004;12:147.
[6] Schölhammer J, Baretzky B, Gust W, Mittemeijer E, Straumal B. Interface Sci 2001;9:43.

[7] Chang L-S, Rabkin E, Straumal BB, Baretzky B, Gust W. Acta Mater 1999;47:4041.
[8] Ference TG, Balluffi RW. Scr Metall 1988;22:1929.
[9] Donald AM, Brown LM. Acta Metall 1979;27:59.
[10] Michael JR, Williams DB. Metall Trans A 1984;15:99.
[11] Straumal BB, Polyakov SA, Bischoff E, Gust W, Mittemeijer EJ. Interface Sci 2001;9:287.
[12] Ernst F, Finnis MW, Koch A, Schmidt C, Straumal B, Gust W. Z Metallkd 1996;87:911.
[13] Alber U, Mullejans H, Rühle M. Acta Mater 1999;47:4047.
[14] Siegl R, Vitek V, Luzzi DE, Yan M. J Phase Equilb 1997;18:562.
[15] Apykhtina I, Bokstein B, Khusnutdinova A, Peteline A, Rakov S. Def Diff Forum 2001;194–199:1331.
[16] Wulff G. Trudy Warsh Obsh Estestvoisp 1894;6:7 [in Russian]; Wulff G. Zeitschrift Kristallogr 1901;34:449 [in German].
[17] Andreev AF. Sov Phys JETP 1981;53:1063.
[18] Rottman C, Wortis M. Phys Rep 1984;103:59; Rottman C, Wortis M. Phys Rev B 1984;29:238.